Corrected: Publisher Correction

The ultrafast X-ray spectroscopic revolution in chemical dynamics

Peter M. Kraus, Michael Zürch, Scott K. Cushing, Daniel M. Neumark and Stephen R. Leone

Abstract | The past two decades have seen rapid developments in short-pulse X-ray sources, which have enabled the study of nuclear and electronic dynamics by ultrafast X-ray spectroscopies with unprecedented time resolution ranging from nanoseconds to attoseconds. In this Perspective, we discuss some of the major achievements in the study of nuclear and electronic dynamics with X-ray pulses produced by high-harmonic, free-electron-laser and synchrotron sources. The particular dynamic processes probed by X-ray radiation highlighted in this Perspective are electronic coherences on attosecond to femtosecond timescales, chemical reactions, such as dissociations, and pericyclic ring-openings, spin-crossover dynamics, ligand-exchange dynamics and structural deformations in excited states. X-ray spectroscopic probing of chemical dynamics holds great promise for the future owing to the ongoing developments of new spectroscopies, such as four-wave mixing, and the continuous improvements in emerging laboratory-based, high-harmonic sources and large-scale, facility-based, free-electron lasers.

Time-resolved experimental techniques have played a major role in our fundamental understanding of chemical processes. Temperature jump[1] and flash photolysis[2] methods were rigorously explored in the 1950s. Their application led to the successful investigation of reactive free radicals and other transient species[2], as well as the study of fast ionic reactions, such as the association of protons and hydroxide to form water[1]. The success of these methods culminated in the 1967 Nobel Prize in Chemistry being awarded to Manfred Eigen, Ronald George Wreyford Norrish and George Porter "For their studies of extremely fast chemical reactions, effected by disturbing the equilibrium by means of very short pulses of energy" (REF.[3]). These studies were mainly concerned with species and reactions occurring on the microsecond to nanosecond timescale and employed only incoherent light sources.

Ultrafast lasers can reveal even faster processes than those occurring at the nanosecond timescale, providing access to the timescales on which a chemical bond forms or breaks. Pump–probe experimental techniques have been developed to record the real-time evolution of photochemical reactions in order to follow nuclear dynamics on the potential energy surfaces of electronically excited molecules[4–7] and to spectroscopically characterize the corresponding transient species[8]. These breakthroughs led to another Nobel Prize in Chemistry, which was awarded in 1999 to Ahmed H. Zewail "For his studies of the transition states of chemical reactions using femtosecond spectroscopy" (REF.[9]).

After a tremendously successful era of studying chemical dynamics, one might ask where the next frontier lies. Considerable efforts are underway to develop techniques to make a 'molecular movie', in which one follows the evolving geometric structure of a molecule undergoing a reaction. X-ray diffraction and scattering[10], as well as electron diffraction methods[11], have been developed to study transient nuclear structures during electrocyclic reactions[10] and photoinduced elimination reactions[11] and to image atomic-scale motion during molecular dissociations[12]. In addition to changes in the arrangement of nuclei, the temporal evolution of the electronic structure can also provide important information on chemical reactivity. Electron dynamics can occur on timescales as fast as attoseconds and can be probed by powerful spectroscopic methods. Possibly, the ultimate goal of studying photochemical reaction dynamics would be to instantly remove or excite an electron in a complex molecule and subsequently follow how the initial photoexcitation triggers the electron dynamics, which resolves into nuclear dynamics and bond breaking. This Perspective outlines how emerging X-ray spectroscopic techniques can be applied to accomplish this challenge and to follow the dynamics of both the electronic and nuclear structure of chemical complexes.

Generally, the probing wavelength in an ultrafast experiment determines which transitions can be detected between the initial and final states of a chemical process and thus what aspects of a reaction are monitored. Many spectroscopic techniques that make use of visible and infrared light have been developed to probe transitions between valence states and vibrational levels, respectively. X-ray spectroscopy, instead, can elucidate the dynamics by probing transitions from a core orbital into a valence state. These localized core-level transitions are element-specific because the energies of the core levels are mostly unaffected by the chemical environment but are sensitive to the local electronic structure. X-ray spectroscopies rely on reporter atoms with characteristic core-to-valence transition energies to follow dynamical processes[13], therefore, resulting in a sensitive tool to follow the charge-state dynamics, oxidation states and spin states of atoms and molecules. This is especially the case when changes in the oxidation state of the atom — and thus the effective screening of the core-hole potential — shift the energies of the core levels during chemical reactions. In favourable cases, the sensitivity of the core-level energies to changes in internuclear separation can even provide direct information about bond length changes[14–16]. If the screening of the core-hole potential does not change much during a dynamical process, the core-level

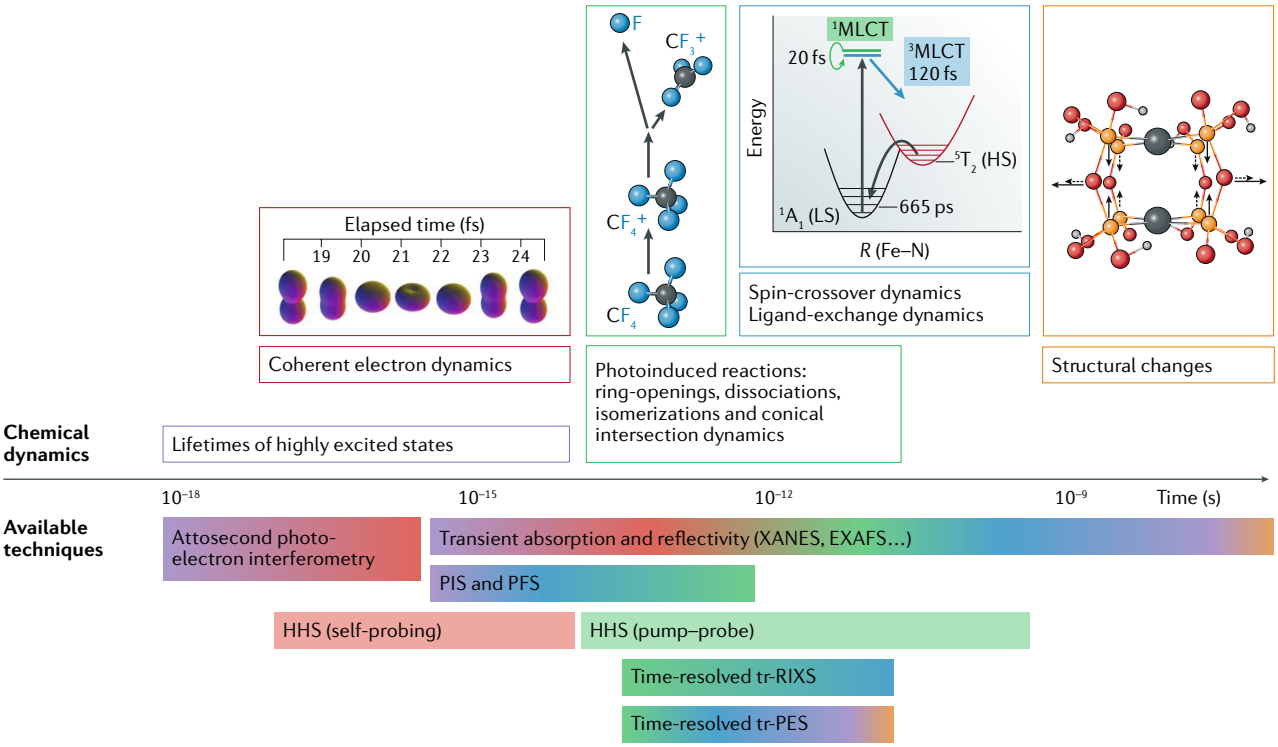

Fig. 1 | **X-ray spectroscopy of chemical dynamics.** Chemical dynamic processes occur on different timescales spanning from attoseconds (10^{-18} s) to nanoseconds (10^{-9} s). Various X-ray techniques are suited to investigate the different processes on all timescales. EXAFS, extended X-ray absorption fine structure; HHS, high-harmonic spectroscopy; HS, high spin; LS, low spin; MLCT state, metal-to-ligand charge-transfer state; PIS, photoion spectroscopy; PFS, photofragmentation spectroscopy; *R*, bond length; tr-PES, time resolved-photoelectron spectroscopy; tr-RIXS, time resolved-resonant inelastic X-ray scattering; XANES, X-ray absorption near-edge structure. Graphics for coherent electron excited states adapted from REF.[46], Macmillan Publishers Limited. Graphics for photoinduced reactions adapted with permission from REF.[72], AAAS. Graphics for spin crossover dynamics and ligand–exchange dynamics adapted with permission from REF.[73], AAAS. Graphics for structural changes adapted with permission from REF.[74], John Wiley and Sons.

energy shifts are negligible compared with the valence-shell dynamics, which can make core-level spectroscopy a selective tool for following valence-shell processes.

Another major advantage in using X-rays to probe chemical dynamics is offered by the possibility to generate shorter pulses in the X-ray spectral region than in the visible spectral region[17]. Synchrotron-based experiments can employ femtosecond slicing techniques to obtain pulse durations in the range of tens to hundreds of femtoseconds[18]. Autocorrelation measurements of X-ray free-electron lasers (FELs) by two-photon ionization have demonstrated pulse durations on the order of 30 fs (REFS[19,20]), and photoelectron streaking measurements revealed X-ray pulses being on average no longer than 4.4 fs (REF.[21]). The latest developments are devoted to decreasing the pulse durations to the sub-femtosecond range, and single-spike hard X-ray pulses with a bandwidth supporting pulse durations of about 200 as have been generated[22]. Attosecond pulses[23] are at the current frontier of ultrashort pulse generation. These can be used to measure purely electronic dynamics before the onset of any nuclear motion. High-harmonic generation (HHG)-based X-ray sources can enable ultrashort pulses with a duration of a few tens of attoseconds[24–28], with the shortest currently reported pulse duration being 43 as (REF.[28]). As opposed to FEL and synchrotron experiments[29,30], which need to be carried out at large-scale facilities, HHG-based experiments have the advantage that they can be realized in a table-top laboratory setting.

In this Perspective, we discuss the photoinduced chemical dynamics that occur over timescales spanning from attoseconds to nanoseconds. Examples of such processes will be presented along with the X-ray techniques used to probe these processes (FIG. 1). This Perspective is not intended as a complete review of all available studies of chemical dynamics with X-rays, but it rather highlights what X-ray spectroscopic methods can contribute to our understanding of chemical dynamics. This Perspective focuses on molecular species, rather than materials, for which X-rays also offer similarly exquisite new determinations of time dynamics[31–40].

X-ray techniques for chemical dynamics

FIGURE 1 illustrates the relevant timescales of photoinduced chemical dynamics and the most prominent X-ray spectroscopic methods with the corresponding achievable time resolution. These techniques are further explained in BOX 1. The fastest processes relevant to chemical dynamics are lifetimes of highly excited states and delays in photoemission[41–43]. The relevant timescales range from several femtoseconds for Auger decays of core-excited states (7.9 fs for the Auger decay of krypton[44]) to only a few attoseconds (<10 as) for the photoemission time delays between the ground and excited shake-up states of helium cations[45]. Attosecond photoelectron interferometry techniques are powerful for measuring such delays. These techniques are based on extreme ultraviolet (XUV) and/or X-ray photoionization and make use of a phase-locked near-infrared pulse to modulate the momentum of the outgoing electron to exactly time its moment of release.

The preparation of a manifold of electronically excited states can initiate coherent electron dynamics. A prerequisite is that the lifetimes of the excited states are

Box 1 | **X-ray spectroscopic methods for following chemical dynamics**

Different X-ray techniques can be used in time-resolved (tr) experiments to measure chemical dynamics, as illustrated in the figure below. The red arrows indicate processes induced by visible (VIS) and/or infrared (IR) pulses, and violet arrows indicate X-ray-induced processes.

tr-XANES (X-ray absorption near-edge structure) spectroscopy
VIS and/or IR pump pulses excite valence electrons, and the photoinduced dynamics are probed by measuring the electron transition from the core to the valence state (VS) by means of broadband X-ray absorption spectroscopy.

EXAFS (extended X-ray absorption fine structure) spectroscopy
X-rays excite an electron from a core level to the valence state, and the excited electron can scatter with neighbouring electrons. This scattering process leads to intensity modulations of the extended X-ray absorption spectrum at energies higher than the core-to-valence electron transition. The modulations imprint the bond lengths between neighbouring atoms.

HHS (high-harmonic spectroscopy)
During the interaction of an intense VIS/IR laser pulse with an atom or molecule, a valence electron is ionized, accelerated and driven back to the parent ion. This leads to the emission of soft X-rays by high-harmonic generation (HHG), which is sensitive to the electronic structure of the atom or molecule. This process can be used for probing electronic and nuclear dynamics in a pump–probe experiment, and can also be used in a unified pump–probe scheme, in which strong-field ionization is the pump process and photorecombination represents the probe process.

tr-PES (photoelectron spectroscopy)
VIS and/or IR pump pulses excite valence electrons, which modify the core-level energies. The dynamics are tracked by ionizing core electrons with X-ray pulses.

tr-RIXS (resonant inelastic X-ray scattering)
VIS and/or IR pump pulses excite valence electrons. The dynamics are measured by exciting a core electron with a narrow-band X-ray pulse to the valence states. The core hole is then re-occupied by another valence electron, which leads to the emission of an X-ray pulse with a different photon energy. The energy difference between the incident and emitted X-rays directly reveals energy-level separations in the valence shell. The re-emission of X-rays with a different energy can also be understood as an inelastic scattering process, hence the name RIXS.

tr-PFS (photofragmentation spectroscopy)
X-ray pump pulses excite inner and outer valence electrons and ionize an AB molecule, and VIS and/or IR probe pulses ionize another electron from the AB^{*+} ion. The photofragmentation products (A^+,B^+ and others) from the doubly ionized molecule AB^{2+} are measured as a function of the pump–probe delay.

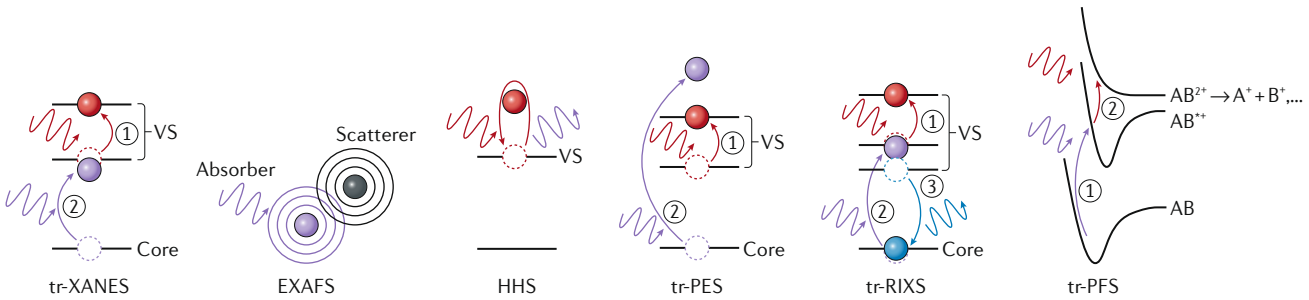

long enough and exceed the duration of one period of the coherent electron dynamics, which is given by the energy separations of the excited states and is typically on the order of a few femtoseconds[46–49]. High-harmonic spectroscopy (HHS) is an X-ray emission technique that can be employed as a unified pump–probe scheme[164]. During HHG, the precisely timed strong-field ionization at a maximum of the peak intensity during every half cycle of a strong laser pulse ionizes the investigated molecule. Subsequently, the ionized electron is accelerated and, when the field reverts its sign, the electron is driven back and can recombine with the parent cation[50,51]. The ionization process can induce both electronic and nuclear dynamics, whereas the photorecombination process can be interpreted as time-reversed photoionization, which strongly depends on the electronic structure of the evolving transient species. In addition, every emitted high-harmonic frequency corresponds to the time that the electron has spent in the continuum[164]. Thus, the energy axis can be converted into a transit-time axis of the continuum electron[52,53]. This allows the process of HHG to be employed as a unified pump–probe scheme. This approach was first used to follow the nuclear motion of the hydrogen atoms in H_2 after strong-field ionization. By comparing the HHG spectra of H_2 and D_2, it was possible to reach a resolution of about 100 as (REF.[51]). This technique has been further developed to follow the periodic relaxation of an electron hole in CO_2 (REF.[54]) and N_2 (REF.[55]), as well as charge migration in HCCI (REF.[48]). Independently, HHS has been demonstrated to be very sensitive to the electronic structure of atoms and molecules through the photorecombination dipole moment. This sensitivity of HHG was used for the tomographic imaging of molecular orbitals[56,57] in spatially aligned molecules and to measure photorecombination resonances[58–60] and laser-modified electronic structures[61]. Moreover, generating high-frequency harmonics with an infrared pulse from a photoexcited sample can be employed as a probe in a pump–probe experiment, which enabled photochemical studies of the dissociation[62,63] of Br_2 and CH_3I, as well as conical intersections of the potential energy surfaces in NO_2 (REFS[64–66]). Recent advances in solid-state HHG[67] have pointed out opportunities to extend this technique for measurements of transient band structure changes[68] and phase transitions in strongly correlated materials[69].

Electronic dynamics and coherences can also be studied by time-resolved X-ray absorption near-edge structure (tr-XANES) spectroscopy. tr-XANES spectroscopy

measures the electronic structure from the viewpoint of a reporter atom in terms of the joint density of states (jDOS) between a core level and an empty valence state. Importantly, the frequency resolution of tr-XANES spectroscopy is not limited by the bandwidth of the laser pulses but by the natural linewidth of the electronic transitions: the measurement of an absorption line can be interpreted as the interference between the X-ray radiation and the induced X-ray polarization[70]. Thus, tr-XANES is a popular technique for investigations on all timescales. Examples in this Perspective include the measurement of coherent electron dynamics[46] on the attosecond to femtosecond timescale, photodissociation and electrocyclic ring-opening dynamics on the timescale of tens to hundreds of femtoseconds[71,72] and spin-crossover dynamics on the femtosecond to picosecond timescale[73].

XANES spectroscopy provides information on the electronic structure from the viewpoint of a reporter atom; however, extensions of this technique to several tens to a hundred eV above the onset of an absorption edge can specifically reveal information on the nuclear structure. The extended X-ray absorption fine structure (EXAFS) arises from the scattering of a photoelectron by neighbouring atoms, in which the intensity modulations are dependent on the arrangement of atoms in the vicinity of the reporter atom[74]. Such structural changes typically occur on shorter timescales (on picosecond to nanosecond timescales), as in the case of structural changes in photoactivated diplatinum complexes, which is discussed below. Typically, EXAFS signals are weak and require the high signal levels provided by synchrotron sources. However, the first EXAFS study with attosecond pulses from a table-top high-harmonic source in graphite was recently demonstrated, opening many future paths for time-resolved studies[165]. As noted, nuclear dynamics can be also studied by means of XANES, through the dependence of the core-level transition energy on the internuclear separation[14–16]. Thus, optical X-ray absorption spectroscopy in the form of XANES or EXAFS can already provide information on all relevant timescales down to attoseconds, with sensitivity to electronic and nuclear dynamics.

X-rays emitted from the sample can also be detected and analysed. In X-ray emission spectroscopy (XES)[75], an X-ray photon is used to create a core hole, and subsequently, X-ray fluorescence or resonant inelastic X-ray scattering (RIXS) processes are detected. X-ray emission is due to the transition of an electron from the valence orbitals to the core hole. It thus provides information on the density of occupied states, as opposed to X-ray absorption, which provides information on unoccupied states. This sensitivity to occupied states was used to track photosynthetic O_2 formation in photosystem II on microsecond timescales and to identify the previously postulated but unobserved S_4 state in the oxygen evolution cycle[76].

Photoemission techniques enable one to directly ionize core electrons instead of observing core-to-valence transitions and to detect electrons instead of photons. This approach has the additional benefit of exclusively tracing the dynamics of charge-state changes and interfacial charge transfer[77,78] through changes in the energies of the core electrons. Techniques based on XUV and X-ray photoemission can be used to follow the dynamics on femtosecond to nanosecond timescales[79–81]. In addition to core-level photoelectron studies, X-rays can be tremendously useful for valence-state photoemission studies. The high photon energies allow one to map a large portion of a material's band structure using angle-resolved photoemission spectroscopy (ARPES)[82]. Time-resolved ARPES with XUV pulses[83,84] generated by HHG for valence-shell photoemission have been successfully applied to measure light-induced phase transitions[85] and to identify the mechanisms of these transitions[86]. New high-repetition-rate, narrow-band HHG sources[87] pave the way towards studies of electron dynamics in novel materials.

Charge transfer following photoexcitation or photoionization can occur on timescales of a few femtoseconds[166] and can be monitored with high temporal resolution through photofragmentation spectroscopy (PFS)[47,88]. This technique was applied to measure charge-transfer dynamics in the phenylalanine cation, in which XUV pulses first ionized phenylalanine and subsequent infrared pulses probed the ionization-induced electronic and nuclear dynamics by ionizing the system to a dication state, which subsequently dissociated[47,89]. The evolution of the yield of the fragment ion as a function of pump–probe delay corresponds to the evolving charge density.

Complicated spin-crossover dynamics can be resolved by XANES spectoscopy[73], but in complex systems, passage through multiple chemically similar transition states cannot always be resolved by simple absorption measurements. RIXS is a new powerful X-ray emission technique that can solve this problem. In RIXS, X-ray pulses are used to excite core electrons in the sample; the core hole is then refilled by a valence electron, and the spectrum of the subsequent X-ray emission is detected as a function of the incident X-ray photon energy. This can be understood as an X-ray scattering technique, which leaves the sample in an excited state and effectively probes valence-shell electron transitions by measuring the energy difference between incident and outgoing photons, minimizing the effect of core-hole shifts. The first time-resolved RIXS studies resolved ligand-exchange and spin-crossover dynamics in an EtOH solution of $Fe(CO)_5$ (REF.[90]), and the results are discussed in detail below.

Before concluding this section, we briefly discuss the technical constraints of different X-ray sources. As mentioned earlier, only HHG sources can be realized in a table-top setting and currently provide the best time resolution[26,28]. Further characteristic and current state-of-the-art parameters of HHG, FEL and synchrotron sources are summarized in TABLE 1. Although HHG sources are hugely advantageous owing to their compactness and

Table 1 | **Overview of available short-pulse X-ray light sources**

Source	Photon energy	Pulse energy	Repetition rate	Average power	Pulse duration
High-harmonic generation	<1.5 keV (REF.[115]); large flux for time-resolved experiments at <450 eV (REFS[71,72,116])	• 10 μJ (at 10 Hz, 20 eV)[156,157] • Typically <1 nJ at 1 kHz (REFS[157–159])	Up to 80 MHz (REF.[160])	• <10 μW (REFS[160,161]) • 1 mW expected[162]	43 as (at 100 eV)[28]
Free-electron laser	<24 keV (0.5 Å)[95,96]	Up to 1 mJ	~100 Hz, 27 kHz and 1 MHz planned[96]	Up to 120 mW (REFS[95,96])	• 4.4 fs (REF.[21]) • Bandwidth supports 200 as (REF.[22])
Synchrotron (time sliced)	<100 keV (REF.[163])	1 nJ (REF.[163])	1–10 kHz (REF.[163])	10 μW (REF.[163])	100 fs (REF.[163])

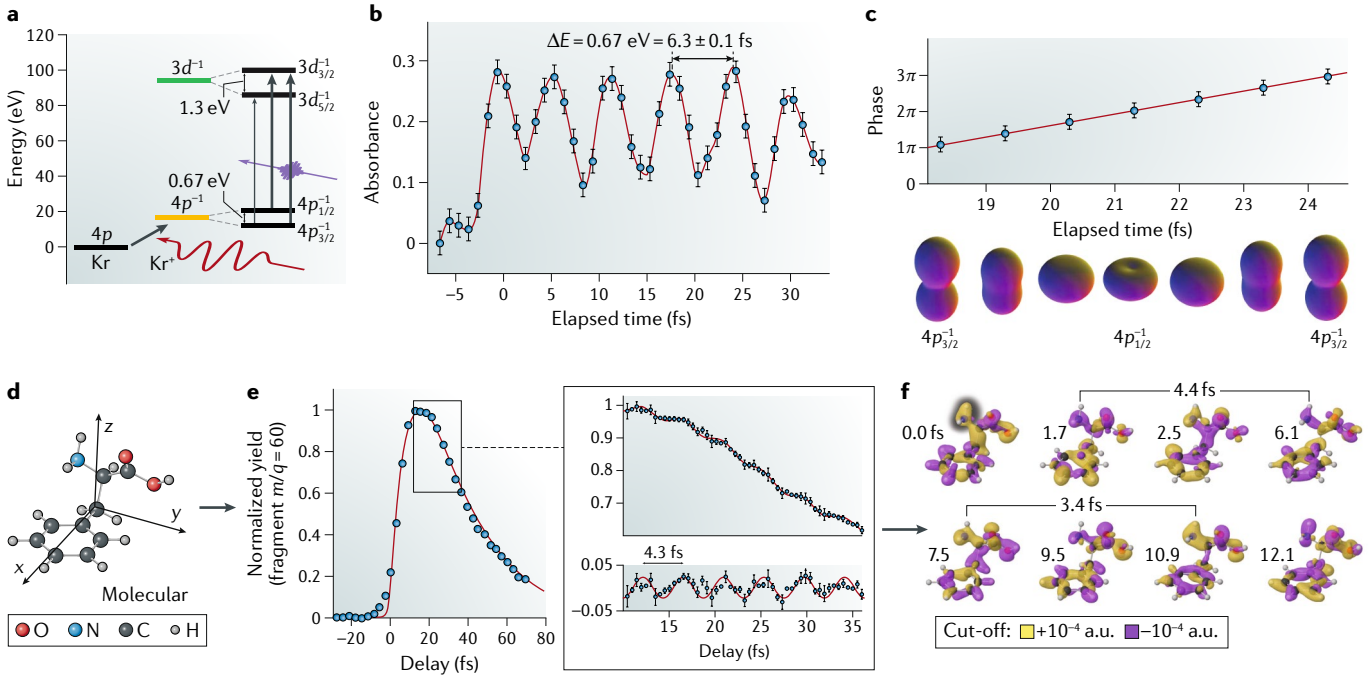

Fig. 2 | **Electronic coherence measured in atoms and molecules.** **a** | Schematic of the 4*p*-shell holes in a Kr ion excited by a visible-light laser pulse. The extreme ultraviolet (XUV) probe, not shown, measures transitions from the 3*d* shell. The energy splitting between the $4p^{-1}_{3/2}$ and $4p^{-1}_{1/2}$ shells is shown. **b** | This energy splitting leads to coherent oscillations, as measured over a photon energy range of 81.20–81.45 eV, corresponding to the $4p^{-1}_{3/2} \rightarrow 3d^{-1}_{3/2}$ transition. **c** | The quantum phase and ensemble-average hole density distributions in the 4*p* sub-shell, as reconstructed from the measured coherence and a density matrix model. This graph illustrates that the full quantum dynamics of ionized xenon in terms of amplitude, phase and extent of coherence can be measured. **d** | Molecular structure of the amino acid phenylalanine. **e** | Measurement of the yield of doubly charged immonium ions following excitation with an attosecond pump pulse. Each data point corresponds to a time step of 3 fs and the fitting curve (red line) corresponds to an exponential increase in the yield during the temporal overlap of the pump and probe pulses, and an exponential decay within the next 55 fs. Data were collected more frequently (every 0.5 fs) during the first 25 fs of the decay period. These data appear in the enlarged region, with the bottom panel showing oscillations of the immonium ion yield due to an electronic coherence with a period of 4.3 fs. **f** | Computed time-averaged hole density following attosecond ionization. The amine group, which is responsible for the oscillations in the yield of the doubly charged immonium ion (shown in panel **e**), is shaded in the first panel. The origin of the measured electronic wavepacket coherence is indicated. Panel **f** provides a theoretical explanation of the experimental observation in panel **e**: XUV ionization induces complex electron dynamics as illustrated in panel **f**, which leads to modulations of the doubly charged immonium ion yield. Panels **a–c** are adapted from REF.[46], Macmillan Publishers Limited. Panels **d–f** are adapted with permission from REF.[47], AAAS.

short pulse durations, their main drawback is the low conversion efficiency (on the order of 10^{-6}) of infrared pules to soft X-rays, resulting in low pulse energies. However, comparatively high average powers on the order of <1 mW for MHz repetition rates can currently be generated by XUV frequency combs, which rely on coupling an infrared frequency comb into an XUV enhancement cavity[91,92]. New high-energy and high-power X-ray sources are currently being developed in the Extreme Light Infrastructure Attosecond Light Pulse Source (ELI-ALPS) facility, which will be the first facility of its kind for HHG experiments[93,94]. FELs can provide much higher pulse energies, up to mJ, but these are currently limited to rather low repetition rates (~100 Hz). The new Linac Coherent Light Source II (LCLS II) and European X-ray free-electron laser (XFEL) FELs will be the first high-repetition-rate FELs at 1 MHz and 27 kHz, respectively[95]. A good summary of the parameters of all FELs operating in the X-ray regime is given on the XFEL homepage[96]. There are now several femtosecond synchrotron sources around the world that enable precise control over the incidental wavelength at high repetition rates, which are favourable for time-resolved experiments. However, the femtosecond slicing technique[18] inherently limits the available pulse energies.

Attosecond coherent electron motion

Electronic coherence refers to the constant phase relation between the electronic wavefunctions of the ground and excited states of an ensemble of molecules. An electronic wavepacket can be created by photoexciting a molecule. The electronic wave packet evolves coherently if the relative quantum phases between the excited electronic states of all individual molecules within the ensemble are given only by the energy separations of the states, and the phase relations are not changed by possible dephasing mechanisms. Electronic coherence can be thought to be a primary quantum response of a system to a short light pulse. After photoexcitation, the quantum states of a system are initially coherent, which leads to an oscillatory evolution of the electron density and related spectroscopic observables. Once the coherences dephase or the photon energy is transferred to other degrees of freedom, the kinetics can be described classically as exponential decay processes for unimolecular reactions, which represent the typical reaction kinetics for photoinduced reactions. Vibronic couplings, such as the coupling between electronically excited states in a molecule and nuclear degrees of freedom, can cause dephasing of an electronic coherence on timescales as fast as 1 fs (REF.[97]). Nevertheless, long-lived coherences exist and have been thought to play a considerable role in light-induced photosynthetic energy transfer[98], which is still a hotly debated topic[99]. The possibility to observe decoherence rates in coherently excited systems also has tremendous applications in quantum information and

quantum computing. Applications in these fields typically aim at creating a binary entangled state that preserves the excited coherence for a given time[100–102].

Attosecond spectroscopy enables the direct tracking of the coherent quantum evolution of systems (FIG. 2). In 2010, a first pioneering experiment investigated the quantum evolution of an electron hole in ionized Kr atoms[46]. In this experiment, a sub-5 fs near-infrared pump pulse was used to strong-field ionize Kr, preparing the cation in the spin–orbit split states with an electron hole in the $4p^{-1}_{3/2}$ and $4p^{-1}_{1/2}$ states, which are split by an energy separation of $\Delta E = 0.67$ eV, corresponding to an oscillation period of the hole density of $\tau = h/\Delta E = 6.3$ fs. This periodic oscillation was probed using attosecond XUV pulses and detected as core-to-valence band transitions in the Kr absorption spectrum (FIG. 2b). The XUV attosecond pulses promoted 3*d* core electrons into the $4p^{-1}_{3/2}$ and $4p^{-1}_{1/2}$ vacancies, which resulted in a periodic modulation of the XUV absorbance as a function of the pump–probe delay owing to the periodically changing alignment of the *p*-hole superposition state. The combined observation of the amplitude and phase of the oscillations allowed the reconstruction of the evolution of the electron-hole density as a function of the pump–probe delay (FIG. 2c).

Coherent attosecond electron dynamics in more complex systems have attracted considerable interest in recent years. Attosecond charge migrations correspond to purely electronic oscillating coherent motions following ionization, as opposed to charge transfers that also involve nuclear motions. Theoretical analyses[103–105] showed that attosecond charge migration in molecules can be linked to strong electron correlations[104,106–109]. Ultrafast electron dynamics following ionization were investigated experimentally by attosecond spectroscopy through photoionization and fragmentation techniques, as in the case of phenylalanine[47] (FIG. 2d). In this case, the XUV attosecond pump pulse removes one electron to ionize the amino acid, and a subsequent near-infrared pulse removes the second electron through multiphoton ionization. This experiment revealed an oscillation over time in the yield of the immonium dication, which is one of the fragmentation products of doubly ionized phenylalanine (FIG. 2e). Comparison to time-dependent density functional theory (TDDFT) simulations related this oscillation to a complex electronic motion (FIG. 2d).

The results for the Kr atom illustrate that the coherent electronic wavepacket lives for a long time[46] and dephases only once the atoms collide in the gas phase, which typically happens on a nanosecond timescale. The coherent electron oscillations in phenylalanine clearly dephase much more rapidly, in about 40 fs (REF.[47]). The reason for this is the redistribution of the electronic excitation into other states by passage through conical intersections mediated by vibronic couplings and, more generally, the dephasing of electronic coherences through nuclear motion. This redistribution of the electronic excitation energy can induce further reactions and more complex chemical dynamics, which are discussed in the next sections.

Femtosecond reaction dynamics

Femtosecond XANES is ideally suited to follow photochemical dynamics. The changes in the electronic environment of a reporter atom during a chemical reaction lead to energy shifts of the absorption edges, which can be employed to track photochemical processes. Pioneering HHG-based experiments studied the femtosecond dynamics of electrocyclic ring-openings and dissociations at the X-ray C K-edge[71,72]. These examples are shown in FIG. 3.

In the first example, 266 nm, 100 fs laser pulses photoexcite cyclohexadiene from its 1A ground state to the 1B excited state, promoting an electron from the 2π orbital (HOMO) to the 1π* orbital (LUMO) (FIG. 3a,b). The system then relaxes to the 1A ground state of open-chain hexatriene following two conical intersections (CI1 and CI2) and through an intermediate 2A transition state, in which the 1π* orbital is doubly occupied and the 2π orbital unoccupied. This evolution is tracked through the transient XANES signal (FIG. 3c), which reveals that the system proceeds within 60 ± 20 fs to the intermediate 2A state (the so-called pericyclic minimum, see FIG. 3) and subsequently decays within 110 ± 60 fs to the 1A ground state of the ring-open hexatriene molecule. In a similar manner, the femtosecond intersystem crossing in acetylacetone can be tracked via X-ray transient absorption at the C K-edge[110].

The second example refers to the use of tr-XANES spectroscopy for the study of photoinduced excitation and dissociation of tetrafluoromethane (FIG. 3d–f). In this case, a strong near-infrared pulse ionizes CF_4 molecules, which subsequently dissociate into CF_3^+ cations and F atoms (FIG. 3e). The dissociation breaks the symmetry of the system and leads to the appearance of a new C X-ray spectral line at lower energies (FIG. 3f). The C K-edge X-ray transition probes the evolution from a tetrahedral C atom to one in a trigonal planar environment. The transient absorption spectrum (FIG. 3f) reflects the changes in the distance of the dissociating C–F bond (FIG. 3d) and the simultaneous relaxation of the coordinates of the other three fluorine atoms.

The versatility of femtosecond XANES was further demonstrated in many other studies, including the detection of vibrational wavepacket evolution in Br_2 following strong-field ionization[14], ring-opening of selenophene induced by strong-field ionization[111], dissociation of dibromomethane and ferrocene induced by ionization[112,113] and the evolution of transition states during the dissociation of methyl iodide[114]. These measurements were performed at element-specific absorption edges in the XUV range between 40–70 eV.

The current limitations of high-harmonic sources are mainly rooted in the low photon flux at high photon energies. Although it is established that HHG radiation can reach energies >1 keV (REF.[115]), X-ray pump–probe studies around 0.30 keV at the C K-edge have only recently been accomplished[71,72,120], and the achievable energies are being continuously pushed to higher values, currently approaching the Ti L-edge around 0.45 keV (REF.[116]). Synchrotrons and FELs are sources that can provide much higher photon energies than those provided by HHG. Although synchrotrons are intrinsically narrow-band sources, the development of femtosecond slicing in 2001 (REF.[18]) enabled synchrotron-based studies with sub-100 fs time resolution. Femtosecond time slicing relies on the energy modulation of an electron beam in an undulator with an ultrashort laser pulse, which allows the generation of femtosecond synchrotron pulses. The first femtosecond X-ray absorption studies with synchrotron sources addressed the photoinduced phase transition in VO_2 (REF.[117]), which could be simultaneously followed at the V L-edge and O K-edge.

The new capabilities of the femtosecond slicing technique were applied to study spin-crossover dynamics. Spin crossover refers to a change of the spin state of a molecular system, generally triggered by photoexcitation, which is a phenomenon largely studied for Fe(II) complexes[118–120]. According to ligand-field theory, the Fe 3*d* orbitals in the metal complex are split

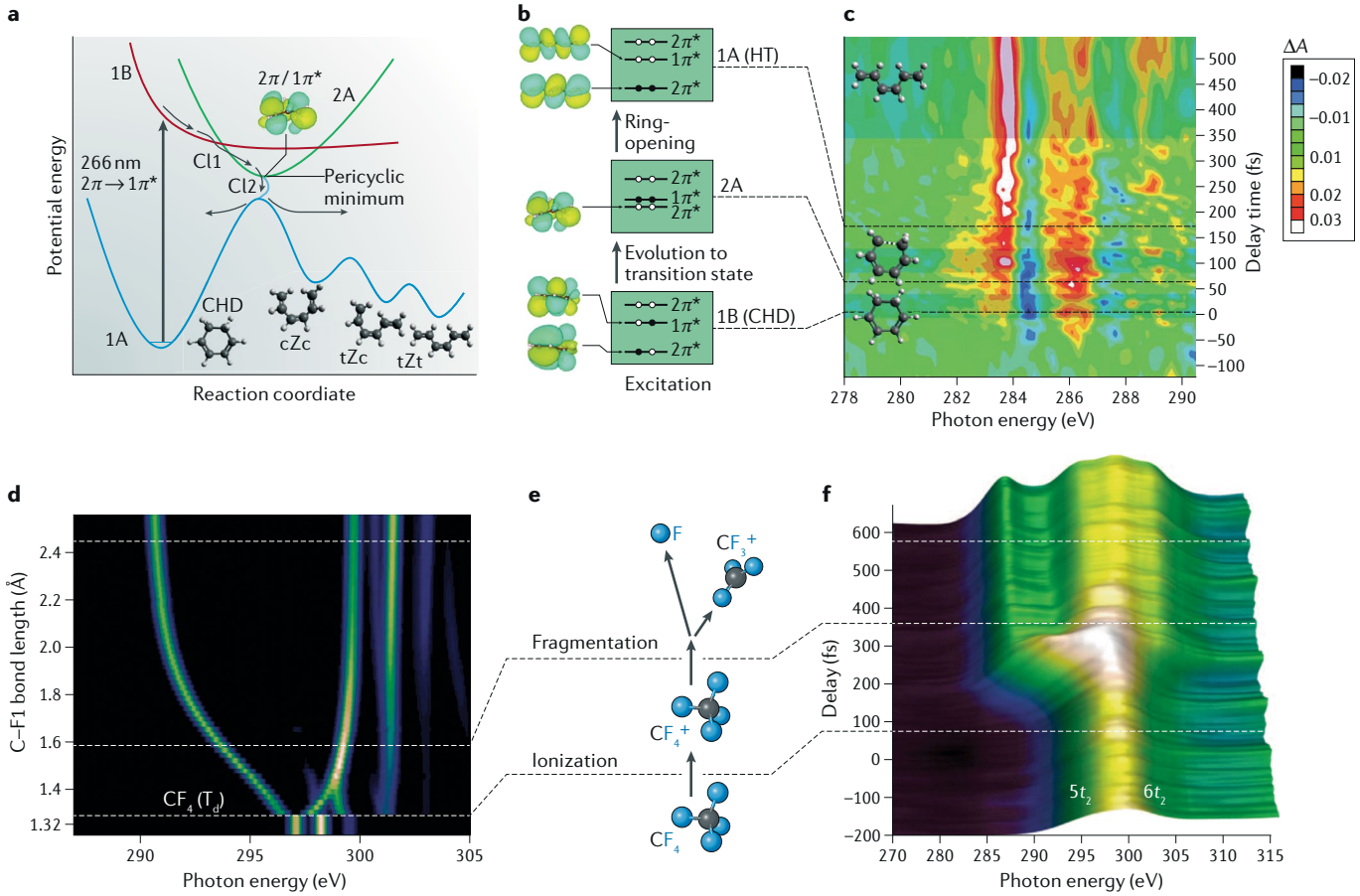

Fig. 3 | **Following a chemical reaction with soft X-ray spectroscopy.** **a** | A schematic view of the potential energy surfaces of ground-state and photoexcited cyclohexadiene (CHD), which undergoes an electrocyclic ring-opening through conical intersections. The ring opening reaction then produces three stereoisomers of 1,3,5-hexatriene (HT): s-*cis*,Z,s-*cis* (cZc); s-*trans*,Z,s-*cis* (tZc,) and s-*trans*,Z,s-*trans* (tZt). **b** | Relevant electronic configurations of the transition states of the photochemical reaction undergone by CHD. **c** | Experimental transient absorption spectrum of CHD in the water window at the carbon K-edge. The transient intensity modulations in the absorption spectrum reflect the population of various transition states during the ring-opening reaction, as illustrated in panel **b**. **d** | Calculated X-ray absorption versus C–F distance for the light-induced $CF_4^+ \rightarrow CF_3^+ + F$ reaction. **e** | Schematic representation of the light induced ionization and fragmentation of CF_4. **f** | Experimental transient absorption spectrum in the water window at the carbon K-edge. The experimental trace in time mirrors the theoretical prediction based on the distance between C and the leaving F. The transient intensity modulations in the absorption spectrum reflect the dissociation reaction, as illustrated in panel **e**. Panels **a–c** adapted with permission from REF.[71], AAAS. Panels **d–f** are adapted with permission from REF.[72], AAAS.

into a triply degenerate t_{2g} set and a doubly degenerate e_g set of orbitals. The 3*d* orbitals are occupied by six valence electrons in the case of Fe(II) and five valence electrons for a photochemically oxidized Fe(III) complex (lower panel in FIG. 4a). If the magnitude of the ligand-field splitting energy is larger than the pairing energy for the electrons, a low-spin (LS) complex is formed, as unpairing the electrons would be energetically unfavourable. By contrast, if the ligand-field splitting energy is lower than the pairing energy, the electrons are unpaired and thus a high-spin (HS) complex is formed. Spin crossover can be induced by light or variations in magnetic fields, temperature or pressure. Generally, spin-crossover complexes can potentially serve as light-induced switches or molecular data-storage devices[121]. Spin-crossover dynamics in the prototypical tris(bipyridine)iron(II)-($[Fe^{II}(bpy)_3]^{2+}$) complex have been studied extensively by ultrafast spectroscopy[118–120]. In particular, the exact relaxation cascade process that leads to the population of the HS state following photoexcitation from the LS state is a debated topic[122]. Femtosecond XANES studies at the Fe K-edge of $[Fe^{II}(bpy)_3]^{2+}$ resolved this controversy[73,123]. The study is summarized in FIG. 4. Pump pulses centred at 266 nm excited the LS ground state to the singlet metal-to-ligand charge-transfer (^{1}MLCT, see FIG. 4a) state, effectively reducing the metal centre. The subsequent structural dynamics can be followed by exploiting the known correlation between the increased XAS peak intensity at the Fe K-edge and the increased Fe–N bond length[73], which led to the determination of different bond lengths for different complexes. Bressler et al.[73] observed a substantial increase in the absorption edge after a relatively long delay of 50 ps (FIG. 4b), indicating the formation of a long-lived HS complex corresponding to a $^5T_2$ quintuplet state, which is the final product of a spin crossover of the photoexcited singlet MLCT state. Thus, time-resolved measurements at the Fe K-edge (7,126 eV) were used to follow the evolution of the bond length after photoexcitation. A step-like rise in the absorbance within 250–300 fs (FIG. 4c) indicated the ultrafast formation of the HS ($^5T_2$) complex. Comparison with a kinetic model confirmed the mechanism to be $^1A_1 + h\nu \rightarrow {}^1$MLCT$\rightarrow {}^3$MLCT$\rightarrow {}^5$T. Although the photoexcitation to the singlet MLCT state is quasi instantaneous, the decay to the triplet state occurs within 20–30 fs and is thus below the experimental time sensitivity

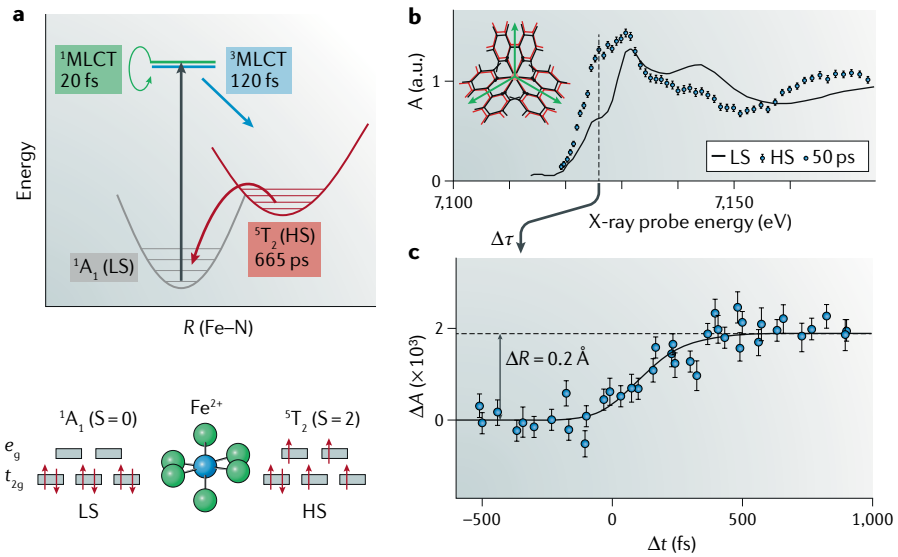

Fig. 4 | **Time-resolved XANES measurement of spin-crossover dynamics in aqueous tris(2,2´-bipyridine)iron(II) ([Fe^{II}(bpy)$_3$]$^{2+}$). a** | Schematic of the potential energy surfaces along the Fe–N bond distance *R* and relaxation cascade following photoexcitation by a 400 nm laser pulse (black arrow). The initial excitation from the low-spin (LS) state $^1A_1$ to the singlet metal-to-ligand charge-transfer (^{1}MLCT) state is followed by an intersystem crossing into the triplet ^{3}MLCT state and subsequent relaxation to the lowest excited quintet or high-spin (HS) $^5T_2$ state with the timescales indicated. **b** | X-ray absorption near-edge structure (XANES) spectra of the LS and HS states of aqueous [Fe^{II}(bpy)$_3$]$^{2+}$, in which absorbance (A) is measured as a function of X-ray probe energy is measured as a function of X-ray probe energy at a pump–probe delay of 50 ps. The spin crossover can be directly studied at the Fe K-edge, where the resulting bond lengthening (indicated in the inset) causes changes in the XANES spectrum, with the greatest changes near the absorption edge at 7,126 eV . **c** | Ultrafast time-resolved measurement by varying the time delay (Δ*t*) at a fixed photon energy of 7,126 eV (as indicated in panel **b**) by employing femtosecond time slicing at a synchrotron allows measurement of the timescale of spin crossover, found to be approximately 250–300 fs, and comparison to model calculations (black solid line) enables determination of the bond lengthening (Δ*R*), found to be 0.2 Å. ΔA, changes in absorbance obtained by subtracting the absorbance of the unexcited spectrum from the absorbance of the excited state spectrum; bpy, bipyridine. Adapted with permission from REF.[73], AAAS.

but could possibly be observed with table-top X-ray high-harmonic sources.

Picosecond photoactivated dynamics

Transition metal complexes can often find application in solar energy conversions, motivating the study of their fundamental chemical reactivity and their femtosecond to picosecond dynamics[124]. Spin-crossover dynamics (discussed in the previous section) and ligand loss upon photoexcitation can generate changes in the electronic and spin structure that can be detected by suitable spectroscopic techniques. If the excited state is long lived, structural changes will also occur, which need to be measured and quantified. In this section, we describe two characteristic examples of such processes: the ligand-exchange dynamics in $Fe(CO)_5$ and structural deformation in a diplatinum complex following photoexcitation, which are investigated by RIXS and EXAFS spectroscopy, respectively. Both experiments were carried out in liquid environments.

In the first experiment (FIG. 5), a free-flowing liquid jet of $Fe(CO)_5$ in ethanol was excited with 266 nm pump pulses[90], which remove a carbonyl ligand and produce $Fe(CO)_4$. RIXS spectra were recorded at the Fe $L_{2,3}$-edge around 710 eV, where core electrons from the 2*p* orbitals are excited into an unoccupied valence state and lower-lying electrons subsequently refill the core hole, causing X-ray emission. The main intensity maximum in a static RIXS spectrum (not shown in FIG. 5) is at 711.5 eV and corresponds to a $2p$-to-$2\pi^*$ excitation with subsequent inelastic scattering to a lower-lying state ($d\pi^7 2\pi^{*1}$ configuration, 5.5 eV energy transfer). A difference RIXS spectrum is shown in FIG. 5a, in which recorded spectra at negative delays (negative delays refer to probe pulses preceeding the pump pulses) were subtracted from the spectra at positive delays. The substantial changes across the spectrum following photoexcitation indicate changes in the electronic and nuclear structures, which mainly occur as a result of changes in the $2p \rightarrow$LUMO resonance energy within the range of 706.5 to 710 eV. Photoexcitation and ligand dissociation leave a hole in a $d\pi$ orbital, which is localized on the metal. The depletion of the ground state upon photoexcitation is apparent in the signal decrease in the green region in FIG. 5a,b, which is located at the same position of the main RIXS signal of unexcited $Fe(CO)_5$ (not shown). In addition, photoexcitation introduces a new transition at lower energies (706.5 eV, excited state and triplet state) owing to the created hole in the HOMO. The excited singlet state is generated briefly during photoexcitation, with a lifetime of 200–300 fs (red region in FIG. 5a,b), either undergoing spin crossover to form an excited triplet (300 fs lifetime, orange region in FIG. 5a,b) or back-coordination with a CO or an EtOH ligand to form vibrationally excited re-ligated $Fe(CO)_5$ or $Fe(CO)_4$EtOH (blue region in FIG. 5a,b). The peak relative to this back-coordination is close to the original RIXS peak (violet region) but slightly shifted, as the newly formed $Fe(CO)_5$ is vibrationally excited. Alternatively, $Fe(CO)_4$EtOH is formed and occurs with a time constant of about 200 fs. Importantly, in this RIXS study, it was possible to spectrally distinguish the singlet and triplet excited states (red and orange regions in FIG. 5a,b), which have similar X-ray absorption but are characterized by different resonant emission features. The resulting mechanism is summarized in FIG. 5c. Upon photoexcitation from the ground state (blue field in FIG. 5c), a ligand is removed, and an excited state is formed (red), which can either undergo re-ligation in about 200 fs or spin crossover in about 300 fs (orange), and subsequently decays back to the ground state on much longer timescales of about 50–100 ps.

Finally, the geometric structure of a complex can change upon photoexcitation to a long-lived excited state. Stroboscopic X-ray diffraction studies of the diplatinum complex $[Pt_2(P_2O_5H_2)_4]^{4-}$ indicate that the Pt–Pt bond shortens when the complex is in the excited state[125]. EXFAS studies can reveal structural changes, as these variations are due to scattering events of the excited photoelectron with neighbouring atoms. Therefore, subsequent EXAFS studies were carried out and revealed a shortening of the Pt–P and Pt–O separations in the excited state but were insensitive to the Pt–Pt bond changes[126–128]. van der Veen et al. followed up on these experiments and excited a diplatinum complex $[Pt_2(P_2O_5H_2)_4]^{4-}$ at 370 nm into the first singlet excited state and probed its geometry through EXAFS by hard X-rays at the Pt L_3-edge (11.5–11.9 keV)[74].

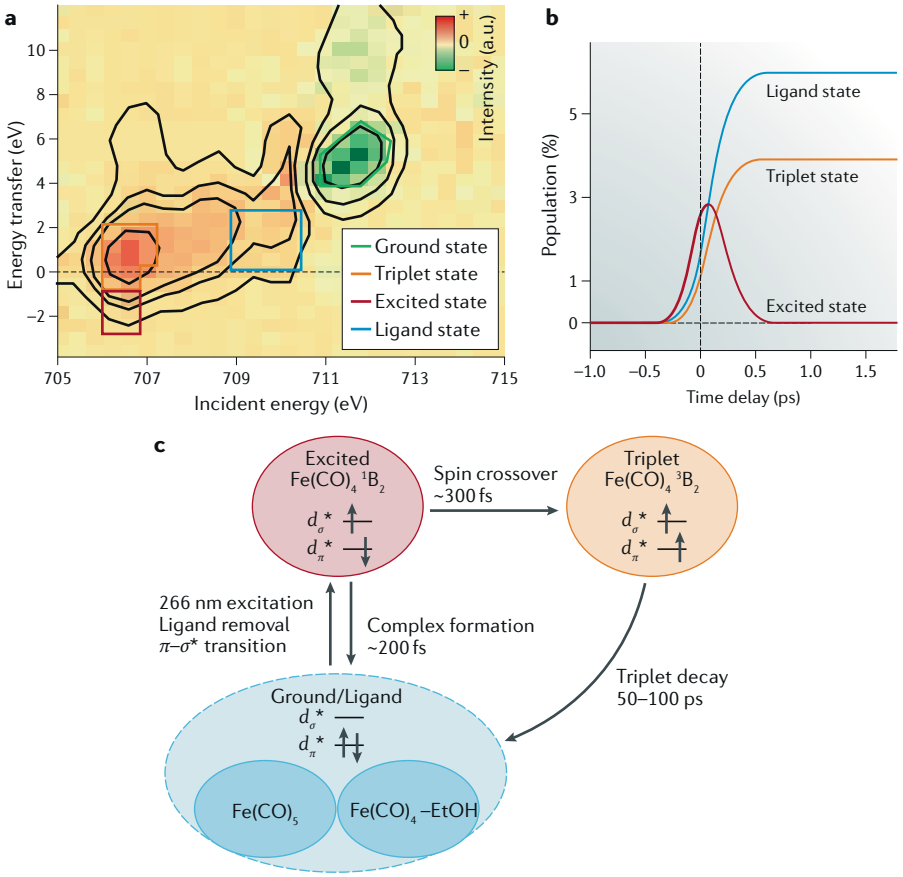

Fig. 5 | **Time-resolved RIXS (free-electron laser) of the ligand-exchange dynamics in aqueous $Fe(CO)_5$. a** | Differential excited-state resonant inelastic X-ray scattering (RIXS) spectrum with highlighted areas of increased and decreased intensity, corresponding to the ground, ligand, excited and triplet state. **b** | From the RIXS map, the excited-state dynamics can be separated into triplet and ligand state contributions. This would not have been possible in an X-ray absorption experiment owing to the overlap of the triplet and excited-state absorption energies. **c** | Inferred excitation and relaxation pathway of the ligand-exchange dynamics following photoexcitation. Adapted from REF.[90], Macmillan Publishers Limited.

Previous studies measuring the metal–metal stretch vibrational frequencies indicated a Pt–Pt bond shortening of 0.175–0.225 Å in the excited state. EXAFS can provide a more direct picture of the global structural changes in the photoexcited complex. Transient EXAFS spectra are shown in FIG. 6, in which the black spectrum shows the ground-state absorption and the red spectrum indicates the excited state. Absorption oscillations versus energy can be predicted from the initial starting geometry of the diplatinum complex, which is iteratively varied to match the experimental spectrum. Following this procedure, the model-based multivariant fitting procedure reveals that the structure of the diplatinum complex is characterized by a 0.31 Å Pt–Pt bond length contraction and a 0.010 Å Pt–ligand elongation. The investigation of bond shortening of dimetal complexes and structural changes by X-ray absorption and scattering techniques remains an active field of research owing to the application of these complexes in catalysis[129–131]. The investigations by EXAFS directly contribute to the determination of the catalytically active studies of these complexes.

Discussion and outlook

In this Perspective, we have described currently available X-ray techniques for the time-resolved spectroscopy of chemical dynamic processes. Attosecond transient absorption and PFS can help to elucidate the evolution of electronic coherences[46,47], which occur on the sub-femtosecond to few-femtosecond timescale. Dephasing of the electronic coherences can trigger more complex molecular processes, and the newly developed capabilities of table-top carbon K-edge transient absorption spectroscopy[71,72,110] (and greater X-ray energy regimes) can be used to study molecular fragmentations and ring-opening reactions. Other pre-eminent dynamical processes, such as spin-crossover[73] and ligand-exchange dynamics[90], occur on similar timescales, and new spectroscopic techniques, such as RIXS, can be used to measure valence energy transfers, reminiscent of the valence energy-level separations and core-level transitions, simultaneously. Finally, EXAFS studies give information on the nuclear dynamics[74].

Synchrotron sources for X-ray spectroscopy have been perfected over the past decades, and HHG-based laboratory sources and FELs are undergoing tremendous improvements. Pulse durations of FELs have been continuously dropping over the past years, and the bandwidths of single-spike pulses are supporting durations of about 200 as (REFS[22,132]), thus approaching the pulse durations achieved by HHG sources. HHG-based XUV and soft X-ray sources already provide the ultimate time resolution, approaching the atomic unit of time (24 as) (REFS[26,28]). Much development is devoted to extending the accessible photon energies to spectroscopically interrogate the C, O and N K-edges, as well as the 3*d* transition metal L-edges. These advances will enable the study of ultrafast charge-transfer and reaction dynamics of novel inorganic materials as well as photochemically active organic and organometallic complexes in gaseous, liquid and solid environments.

The FEL and synchrotron studies on spin crossover and the electronic and structural dynamics of photochemically activated species reported in this Perspective were performed in liquid environments. Soft X-ray studies with high-harmonic sources have been hindered for a long time by the short penetration depths in liquids and solutes.

However, experimental techniques on free-flowing thin liquid jets in a vacuum have made tremendous progress[133–136]. The first high-harmonic-based soft X-ray photoelectron studies were performed on liquid samples[137], and additional studies, including transient absorption experiments, will follow in the future, which will improve our understanding of both the electronic and nuclear dynamics of large and complex molecules.

X-ray spectroscopies are also undergoing rapid technical development, in particular as a result of the developments of new FELs, and higher-flux, higher-photon-energy HHG sources. New FEL sources are being developed in the United States (LCLS II), the European Union (XFFEL in Germany), Switzerland (SwissFEL) and South Korea (Pohang Accelerator Laboratory X-ray Free Electron Laser PAL-XFEL) (for a comparison of available X-ray FEL sources, see the European XFEL facilities comparison), which will deliver brighter and higher-flux

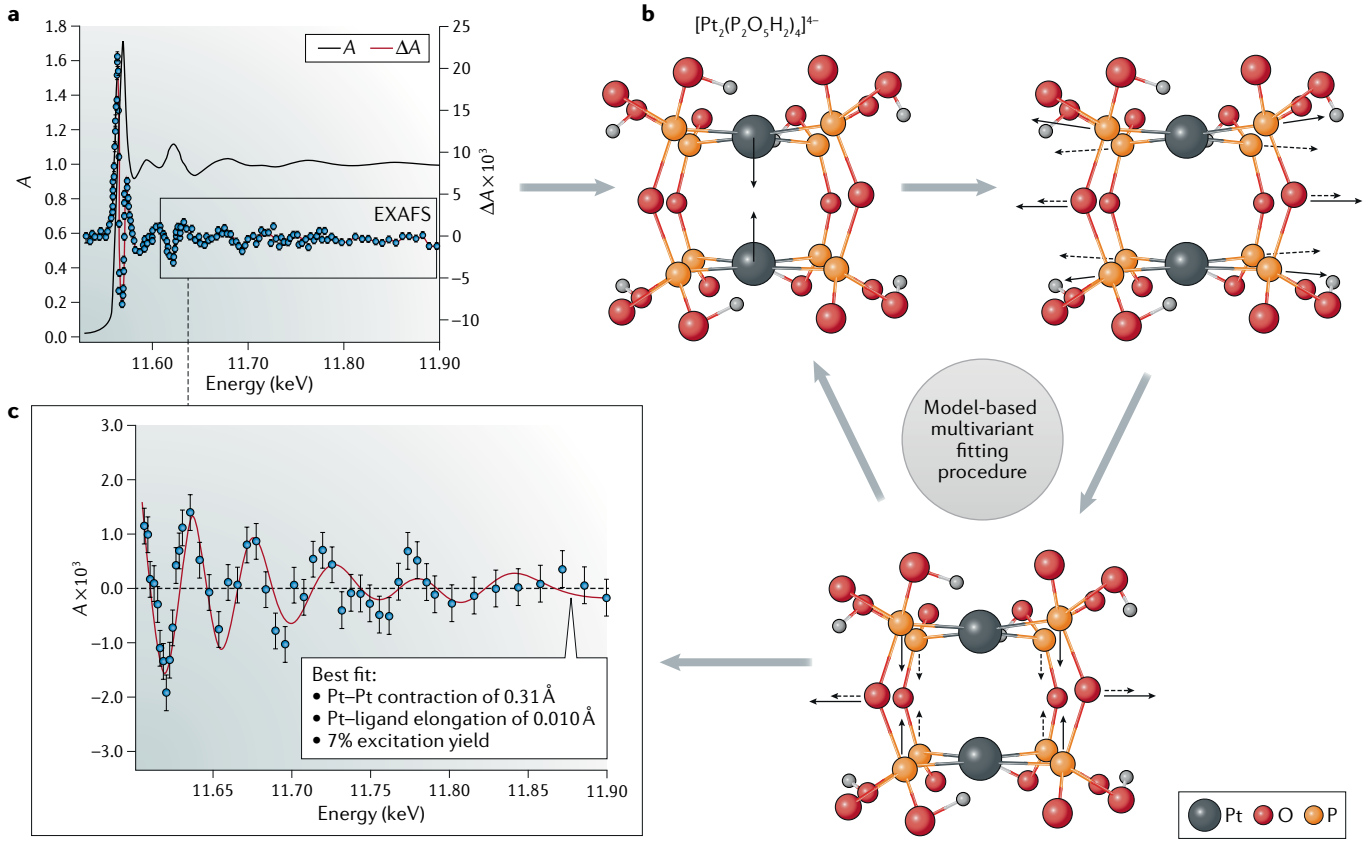

Fig. 6 | **Time-resolved EXAFS measurement reveals structural dynamics of a photochemically active diplatinum molecule in solution.** **a**| Time-resolved extended X-ray absorption fine structure (EXAFS) spectrum is recorded at the platinum L_3 edge (ground-state absorbance in black) 150 ns following photoexcitation with 390 nm light (blue data points, and black curve). The red curve corresponds to the transient absorption (ΔA) that is obtained subtracting the absorption of the excited species from that of the unexcited one. **b,c** | Using a set of likely bond-deformation scenarios, the EXAFS spectrum is calculated and fitted to the experimental data (red line in panel **c**). The excellent agreement with the feature-rich EXAFS spectrum gives insight into bond-deformation dynamics in complex aqueous molecules. Adapted with permission from REF.[74], John Wiley and Sons.

hard X-ray pulses[95]. The femtosecond technology underlying HHG is currently undergoing a rapid change. For the past 20 years, Ti:sapphire lasers delivering 800 nm pulses have been the de facto sources of high harmonics in the XUV and soft X-ray range; however, optical parametric chirped-pulse amplifiers (OPCPAs) are now challenging the pivotal role of Ti:sapphire systems. OPCPAs are capable of producing much higher average powers than Ti:sapphire systems and can benefit the available pulse energies and repetition rates for driving HHG[138]. Additionally, OPCPAs have the advantage of wavelength tunability, which could enable the generation of photon energies up to 1 keV at high fluxes with HHG sources.

The high spatial coherence of the described X-ray sources have opened new paths for imaging nanoscale targets and probing their dynamics with femtosecond time resolution. Transient states of Xe nanoparticles were imaged by looking at the X-ray scattering generated by FEL lasers[139], and single He nanodroplets were imaged through the use of a high-harmonic source[140]. These experiments have paved the way towards nanoscale imaging experiments with few-femtosecond to attosecond time resolution. Such scattering techniques are crucial for studying the initial steps of heterogeneous catalytic reaction cycles[141] of molecules on nanostructured surfaces.

The recent development of table-top high-harmonic sources with circular polarization[34,142] enable soft X-ray experiments on magnetic materials[143] and chiral molecules[144]. Such sources can even be combined with the previously mentioned scattering techniques on nanostructured samples[145], which have been used to image magnetic domains and will enable the investigation of the demagnetization dynamics of structured magnetic materials.

A major driving force behind the construction of FELs is our desire to image biomolecular systems, such as proteins, by femtosecond X-ray nanocrystallography[146]. However, the high intensities required for such imaging experiments induce multiple ionization events and subsequent fragmentation of the proteins[147], which requires the use of very short pulses with durations of a few femtoseconds, as well as a thorough understanding of the ionization dynamics upon X-ray exposure.

Pioneering experiments have investigated the formation of highly charged Ne ions after X-ray exposure[148]. Future experiments could use core ionization to trigger ultrafast sub-femtosecond charge migration[149], which could be probed with element specificity by broadband attosecond absorption measurements.

Further development of high-brilliance sources and attosecond multi-pulse experiments will enable novel X-ray multidimensional spectroscopy. Theoretical research has already explored numerous opportunities[150], and the first four-wave mixing experiments (XUV + two near-infrared photons) were successfully implemented for the study of noble gases[151–153]. Nonlinear X-ray interactions have also been experimentally observed in solids: hard X-ray and optical sum-frequency[154] generation as well as soft X-ray surface second-harmonic

generation[155] have been demonstrated using FELs. Interactions with hard X-rays induce second-harmonic and sum-frequency generation even in centro-symmetric bulk materials owing to optically induced charge fields arising in the exposed sample. On the other hand, soft X-ray surface second-harmonic generation can be a true interface probe owing to the longer wavelength, much like optical surface second-harmonic generation spectroscopy, and will provide a new route for studying ultrafast interface dynamics. In general, multidimensional X-ray techniques have the potential to elegantly separate core-level shifts from valence-shell dynamics and to correlate the induced chemical dynamics to the local environment of single atoms in molecules. As such, multidimensional X-ray techniques can bring another revolution to the studies of chemical dynamics and chemical structure, much like multidimensional NMR, infrared and visible techniques have provided fundamental new insight into chemical science.

Peter M. Kraus[1,2,4], Michael Zürch[1,2], Scott K. Cushing[1,3], Daniel M. Neumark[1,3]* and Stephen R. Leone[1,2,3]**

[1]*Department of Chemistry, University of California, Berkeley, CA, USA.*

[2]*Department of Physics, University of California, Berkeley, CA, USA.*

[3]*Chemical Sciences Division, Lawrence Berkeley National Laboratory, Berkeley, CA, USA.*

[4]*Advanced Research Center for Nanolithography, Amsterdam, Netherlands.*

*e-mail: kraus@arcnl.nl; dneumark@berkeley.edu; srl@berkeley.edu

https://doi.org/10.1038/s41570-018-0008-8

Published online: 29 May 2018

1. Eigen, M. Methods for investigation of ionic reactions in aqueous solutions with half-times as short as 10–19 sec. application to neutralization and hydrolysis reactions. *Discuss. Faraday Soc.* **17**, 194–205 (1954).
2. Porter, G. The absorption spectroscopy of substances of short life. *Discuss. Faraday Soc.* **9**, 60–69 (1950).
3. [No authors listed.] The Nobel Prize in Chemistry 1967. *Nobelprize.org* https://www.nobelprize.org/nobel_prizes/chemistry/laureates/1967/ (2018).
4. Dantus, M., Rosker, M. J. & Zewail, A. H. Real-time femtosecond probing of transition states in chemical reactions. *J. Chem. Phys.* **87**, 2395–2397 (1987).
5. Rosker, M. J., Dantus, M. & Zewail, A. H. Femtosecond clocking of the chemical bond. *Science* **241**, 1200–1202 (1988).
6. Rose, T. S., Rosker, M. J. & Zewail, A. H. Femtosecond real-time probing of reactions. iv. the reactions of alkali halides. *J. Chem. Phys.* **91**, 7415–7436 (1989).
7. Mokhtari, A., Cong, P., Herek, J. & Zewail, A. Direct femtosecond mapping of trajectories in a chemical reaction. *Nature* **348**, 225–227 (1990).
8. Dantus, M., Bowman, R. M., Gruebele, M. & Zewail, A. H. Femtosecond real-time probing of reactions. v. the reaction of IHgI. *J. Chem. Phys.* **91**, 7437–7450 (1989).
9. [No authors listed.] The Nobel Prize in Chemistry 1999. *Nobelprize.org* https://www.nobelprize.org/nobel_prizes/chemistry/laureates/1999/ (2018).
10. Minitti, M. et al. Imaging molecular motion: femtosecond X-ray scattering of an electro-cyclic chemical reaction. *Phys. Rev. Lett.* **114**, 255501 (2015).
11. Ihee, H. et al. Direct imaging of transient molecular structures with ultrafast diffraction. *Science* **291**, 458–462 (2001).
12. Glownia, J. M. et al. Self-referenced coherent diffraction X-ray movie of Ångstrom-and femtosecond-scale atomic motion. *Phys. Rev. Lett.* **117**, 153003 (2016).
13. Loh, Z.-H. & Leone, S. R. Capturing ultrafast quantum dynamics with femtosecond and attosecond X-ray core-level absorption spectroscopy. *J. Phys. Chem. Lett.* **4**, 292–302 (2013).
14. Hosler, E. R. & Leone, S. R. Characterization of vibrational wave packets by core-level high-harmonic transient absorption spectroscopy. *Phys. Rev. A* **88**, 023420 (2013).
15. Dutoi, A. D. & Leone, S. R. Simulation of X-ray transient absorption for following vibrations in coherently ionized F_2 molecules. *Chem. Phys.* **482**, 249–264 (2017).
16. Wei, Z. et al. Elucidating the origins of multimode vibrational coherences of polyatomic molecules induced by intense laser fields. *Nat. Commun.* **8**, 735 (2017).
17. Ramasesha, K., Leone, S. R. & Neumark, D. M. Real-time probing of electron dynamics using attosecond time-resolved spectroscopy. *Annu. Rev. Phys. Chem.* **67**, 41–63 (2016).
18. Schoenlein, R. et al. Generation of femtosecond pulses of synchrotron radiation. *Science* **287**, 2237–2240 (2000).
19. Mitzner, R. et al. Direct autocorrelation of soft-X-ray free-electron-laser pulses by time- resolved two-photon double ionization of he. *Phys. Rev. A* **80**, 025402 (2009).
20. Moshammer, R. et al. Second-order autocorrelation of XUV FEL pulses via time resolved two-photon single ionization of He. *Opt. Express* **19**, 21698–21706 (2011).
21. Helml, W. et al. Measuring the temporal structure of few-femtosecond free-electron laser X-ray pulses directly in the time domain. *Nat. Photon.* **8**, 950 (2014).
22. Huang, S. et al. Generating single-spike hard X-ray pulses with nonlinear bunch compression in free-electron lasers. *Phys. Rev. Lett.* **119**, 154801 (2017).
23. Hentschel, M. et al. Attosecond metrology. *Nature* **414**, 509–513 (2001).
24. Goulielmakis, E. et al. Single-cycle nonlinear optics. *Science* **320**, 1614–1617 (2008).
25. Zhao, K. et al. Tailoring a 67 attosecond pulse through advantageous phase-mismatch. *Opt. Lett.* **37**, 3891–3893 (2012).
26. Li, J. et al. 53-attosecond X-ray pulses reach the carbon K-edge. *Nat. Commun.* **8**, 186 (2017).
27. Cousin, S. L. et al. Attosecond streaking in the water window: a new regime of attosecond pulse characterization. *Phys. Rev. X* **7**, 041030 (2017).
28. Gaumnitz, T. et al. Streaking of 43-attosecond soft-X-ray pulses generated by a passively CEP-stable mid-infrared driver. *Opt. Express* **25**, 27506–27518 (2017).
29. Chen, L. X. Probing transient molecular structures in photochemical processes using laser-initiated time-resolved X-ray absorption spectroscopy. *Annu. Rev. Phys. Chem.* **56**, 221–254 (2005).
30. Chen, L., Zhang, X. & Shelby, M. Recent advances on ultrafast X-ray spectroscopy in the chemical sciences. *Chem. Sci.* **5**, 4136–4152 (2014).
31. Chan, L.-O. et al. Ultrafast demagnetization dynamics at the M edges of magnetic elements observed using a tabletop high-harmonic soft X-ray source. *Phys. Rev. Lett.* **103**, 257402 (2009).
32. Schultze, M. et al. Attosecond band-gap dynamics in silicon. *Science* **346**, 1348–1352 (2014).
33. Jiang, C.-M. et al. Characterization of photo-induced charge transfer and hot carrier relaxation pathways in spinel cobalt oxide (Co_3O_4). *J. Phys. Chem. C* **118**, 22774–22784 (2014).
34. Kfir, O. et al. Generation of bright phase-matched circularly-polarized extreme ultraviolet high harmonics. *Nat. Photon.* **9**, 99–105 (2015).
35. Gierz, I. et al. Tracking primary thermalization events in graphene with photoemission at extreme time scales. *Phys. Rev. Lett.* **115**, 086803 (2015).
36. Lucchini, M. et al. Attosecond dynamical Franz-Keldysh effect in polycrystalline diamond. *Science* **353**, 916–919 (2016).
37. Zürch, M. et al. Direct and simultaneous observation of ultrafast electron and hole dynamics in germanium. *Nat. Commun.* **8**, 15734 (2017).
38. Jager, M. F. et al. Tracking the insulator-to-metal phase transition in Vo_2 with few-femtosecond extreme UV transient absorption spectroscopy. *Proc. Natl Acad. Sci.* **114**, 9558–9563 (2017).
39. Carneiro, L. M. et al. Excitation-wavelength-dependent small polaron trapping of photoexcited carriers in α-Fe_2O_3. *Nat. Mater.* **16**, 819–825 (2017).
40. Moulet, A. et al. Soft X-ray excitonics. *Science* **357**, 1134–1138 (2017).
41. Cavalieri, A. L. et al. Attosecond spectroscopy in condensed matter. *Nature* **449**, 1029 (2007).
42. Schultze, M. et al. Delay in photoemission. *Science* **328**, 1658–1662 (2010).
43. Tao, Z. et al. Direct time-domain observation of attosecond final-state lifetimes in photoemission from solids. *Science* **353**, 62 (2016).
44. Drescher, M. et al. Time-resolved atomic inner-shell spectroscopy. *Nature* **419**, 803 (2002).
45. Ossiander, M. et al. Attosecond correlation dynamics. *Nat. Phys.* **13**, 280–285 (2017).
46. Goulielmakis, E. et al. Real-time observation of valence electron motion. *Nature* **466**, 739–743 (2010).
47. Calegari, F. et al. Ultrafast electron dynamics in phenylalanine initiated by attosecond pulses. *Science* **346**, 336–339 (2014).
48. Kraus, P. M. et al. Measurement and laser control of attosecond charge migration in ionized iodoacetylene. *Science* **350**, 790–795 (2015).
49. Wang, H. et al. Attosecond time-resolved autoionization of argon. *Phys. Rev. Lett.* **105**, 143002 (2010).
50. Lein, M. Attosecond probing of vibrational dynamics with high-harmonic generation. *Phys. Rev. Lett.* **94**, 053004 (2005).
51. Baker, S. et al. Probing proton dynamics in molecules on an attosecond time scale. *Science* **312**, 424 (2006).
52. Corkum, P. B. Plasma perspective on strong field multiphoton ionization. *Phys. Rev. Lett.* **71**, 1994 (1993).
53. Lewenstein, M., Balcou, P., Ivanov, M. Y., L'Huillier, A. & Corkum, P. Theory of high-harmonic generation by low-frequency laser fields. *Phys. Rev. A* **49**, 2117 (1994).
54. Smirnova, O. et al. High harmonic interferometry of multi-electron dynamics in molecules. *Nature* **460**, 972–977 (2009).
55. Haessler, S. et al. Attosecond imaging of molecular electronic wavepackets. *Nat. Phys.* **6**, 200–206 (2010).
56. Itatani, J. et al. Tomographic imaging of molecular orbitals. *Nature* **432**, 867–871 (2004).
57. Vozzi, C. et al. Generalized molecular orbital tomography. *Nat. Phys.* **7**, 822–826 (2011).
58. Wo¨rner, H. J., Niikura, H., Bertrand, J. B., Corkum, P. B. & Villeneuve, D. M. Observation of electronic structure minima in high-harmonic generation. *Phys. Rev. Lett.* **102**, 103901 (2009).
59. Shiner, A. D. et al. Probing collective multi-electron dynamics in xenon with high-harmonic spectroscopy. *Nat. Phys.* **7**, 464–467 (2011).
60. Kraus, P. M., Baykusheva, D. & Wörner, H. J. Two-pulse field-free orientation reveals anisotropy of molecular shape resonance. *Phys. Rev. Lett.* **113**, 023001 (2014).
61. Kraus, P. M. et al. Observation of laser-induced electronic structure in oriented polyatomic molecules. *Nat. Commun.* **6**, 7039 (2015).
62. Wörner, H. J., Bertrand, J. B., Kartashov, D. V., Corkum, P. B. & Villeneuve, D. M. Following a chemical reaction using high-harmonic interferometry. *Nature* **466**, 604–607 (2010).
63. Tehlar, A. & Wörner, H. J. Time-resolved high-harmonic spectroscopy of the photodissociation of CH_3I and CF_3I. *Mol. Phys.* **111**, 2057–2067 (2013).
64. Wörner, H. J. et al. Conical intersection dynamics in NO_2 probed by homodyne high-harmonic spectroscopy. *Science* **334**, 208–212 (2011).
65. Kraus, P. M. et al. Time-resolved high-harmonic spectroscopy of nonadiabatic dynamics in NO_2. *Phys. Rev. A* **85**, 043409 (2012).
66. Kraus, P. M. & Wörner, H. J. Time-resolved high-harmonic spectroscopy of valence electron dynamics. *Chem. Phys.* **414**, 32–44 (2013).
67. Ghimire, S. et al. Observation of high-order harmonic generation in a bulk crystal. *Nat. Phys.* **7**, 138–141 (2011).
68. Vampa, G. et al. All-optical reconstruction of crystal band structure. *Phy. Rev. Lett.* **115**, 193603 (2015).
69. Silva, R., Blinov, I. V., Rubtsov, A. N., Smirnova, O. & Ivanov, M. High harmonic imaging of ultrafast many-body dynamics in strongly correlated systems. *Preprint arXiv* **1704**.08471 (2017).

70. Beck, A. R., Neumark, D. M. & Leone, S. R. Probing ultrafast dynamics with attosecond transient absorption. *Chem. Phys. Lett.* **624**, 119–130 (2015).
71. Attar, A. R. et al. Femtosecond X-ray spectroscopy of an electrocyclic ring-opening reaction. *Science* **356**, 54–59 (2017).
72. Pertot, Y. et al. Time-resolved X-ray absorption spectroscopy with a water window high- harmonic source. *Science* **355**, 264–267 (2017).
73. Bressler, C. et al. Femtosecond xanes study of the light-induced spin crossover dynamics in an iron(II) complex. *Science* **323**, 489–492 (2009).
74. van der Veen, R. M. et al. Structural determination of a photochemically active diplatinum molecule by time-resolved EXAFS spectroscopy. *Angew. Chem. Int. Ed.* **48**, 2711–2714 (2009).
75. Bergmann, U. & Glatzel, P. X-ray emission spectroscopy. *Photosynth. Res.* **102**, 255 (2009).
76. Haumann, M. et al. Photosynthetic O_2 formation tracked by time-resolved X-ray experiments. *Science* **310**, 1019–1021 (2005).
77. Vaida, M. E. & Leone, S. R. Femtosecond extreme ultraviolet photoemission spectroscopy: observation of ultrafast charge transfer at the n-TiO_2/p-Si (100) interface with controlled TiO_2 oxygen vacancies. *J. Phys. Chem. C* **120**, 2769–2776 (2016).
78. Marsh, B. M., Vaida, M. E., Cushing, S. K., Lamoureux, B. R. & Leone, S. R. Measuring the surface photovoltage of a Schottky barrier under intense light conditions: Zn/p-Zi (100) by laser time-resolved extreme ultraviolet photoelectron spectroscopy. *J. Phys. Chem. C* **121**, 21904–21912 (2017).
79. Siefermann, K. R. et al. Atomic-scale perspective of ultrafast charge transfer at a dye–semiconductor interface. *J. Phys. Chem. Lett.* **5**, 2753–2759 (2014).
80. Arion, T. et al. Site-specific probing of charge transfer dynamics in organic photovoltaics. *Appl. Phys. Lett.* **106**, 121602 (2015).
81. Neppl, S. & Gessner, O. Time-resolved X-ray photoelectron spectroscopy techniques for the study of interfacial charge dynamics. *J. Electron. Spectrosc. Related Phenomena* **200**, 64–77 (2015).
82. Gray, A. et al. Probing bulk electronic structure with hard X-ray angle-resolved photoemission. *Nat. Mater.* **10**, 759–764 (2011).
83. Mathias, S. et al. Angle-resolved photoemission spectroscopy with a femtosecond high harmonic light source using a two-dimensional imaging electron analyzer. *Rev. Sci Instruments* **78**, 083105 (2007).
84. Eich, S. et al. Time-and angle-resolved photoemission spectroscopy with optimized high- harmonic pulses using frequency-doubled Ti: Sapphire lasers. *J. Electron. Spectrosc. Related Phenomena* **195**, 231–236 (2014).
85. Rohwer, T. et al. Collapse of long-range charge order tracked by time-resolved photoemission at high momenta. *Nature* **471**, 490–493 (2011).
86. Hellmann, S. et al. Time-domain classification of charge-density-wave insulators. *Nat. Commun.* **3**, 1069 (2012).
87. Wang, H. et al. Bright high-repetition-rate source of narrowband extreme-ultraviolet harmonics beyond 22 eV. *Nat. Commun.* **6**, 7459 (2015).
88. Belshaw, L. et al. Observation of ultrafast charge migration in an amino acid. *J. Phys. Chem. Lett.* **3**, 3751–3754 (2012).
89. Sansone, G. et al. Electron localization following attosecond molecular photoionization. *Nature* **465**, 763–766 (2010).
90. Wernet, P. et al. Orbital-specific mapping of the ligand exchange dynamics of $Fe(Co)_5$ in solution. *Nature* **520**, 78–81 (2015).
91. Jones, R. J., Moll, K. D., Thorpe, M. J. & Ye, J. Phase-coherent frequency combs in the vacuum ultraviolet via high-harmonic generation inside a femtosecond enhancement cavity. *Phys. Rev. Lett.* **94**, 193201 (2005).
92. Pupeza, I. et al. Compact high-repetition-rate source of coherent 100 eV radiation. *Nat. Photon.* **7**, 608 (2013).
93. Charalambidis, D. et al. in The European Conference on Lasers and Electro-Optics CG_4_1 (Munich, Germany, 2013).
94. Kühn, S. et al. The eli-alps facility: the next generation of attosecond sources. *J. Phys. B Atom. Mol. Opt. Phys.* **50**, 132002 (2017).
95. Young, L. et al. Roadmap of ultrafast X-ray atomic and molecular physics. *J. Phys. B Atom. Mol. Opt. Phys.* **51**, 032003 (2018).
96. [No authors listed.] In Comparison. The European XFEL in international comparison. European XFEL https://www.xfel.eu/facility/comparison/index_eng.html (2018).
97. Arnold, C., Vendrell, O. & Santra, R. Electronic decoherence following photoionization: full quantum-dynamical treatment of the influence of nuclear motion. *Phys. Rev. A* **95**, 033425 (2017).
98. Engel, G. S. et al. Evidence for wavelike energy transfer through quantum coherence in photosynthetic systems. *Nature* **446**, 782–786 (2007).
99. Scholes, G. D. et al. Using coherence to enhance function in chemical and biophysical systems. *Nature* **543**, 647 (2017).
100. Shor, P. W. Scheme for reducing decoherence in quantum computer memory. *Phys. Rev. A* **52**, R2493 (1995).
101. Cirac, J. I. & Zoller, P. Quantum computations with cold trapped ions. *Phys. Rev. Lett.* **74**, 4091 (1995).
102. Loss, D. & DiVincenzo, D. P. Quantum computation with quantum dots. *Phys. Rev. A* **57**, 120 (1998).
103. Cederbaum, L. & Zobeley, J. Ultrafast charge migration by electron correlation. *Chem. Phys. Lett.* **307**, 205–210 (1999).
104. Breidbach, J. & Cederbaum, L. S. Migration of holes: formalism, mechanisms and illustrative applications. *J. Chem. Phys.* **118**, 3983 (2003).
105. Remacle, F. & Levine, R. D. An electronic time scale in chemistry. *PNAS* **103**, 6793–6798 (2006).
106. Breidbach, J. & Cederbaum, L. S. Universal attosecond response to the removal of an electron. *Phys. Rev. Lett.* **94**, 033901 (2005).
107. Sansone, G., Pfeifer, T., Simeonidis, K. & Kuleff, A. I. Electron correlation in real time. *ChemPhysChem* **13**, 661–680 (2012).
108. Kuleff, A. I., Lünnemann, S. & Cederbaum, L. S. Electron-correlation-driven charge migration in oligopeptides. *Chem. Phys.* **414**, 100–105 (2013).
109. Kuleff, A. I. & Cederbaum, L. S. Ultrafast correlation-driven electron dynamics. *J. Phys. B Atom. Mol. Opt. Phys.* **47**, 124002 (2014).
110. Bhattacherjee, A., Pemmaraju, C. D., Schnorr, K., Attar, A. R. & Leone, S. R. Ultrafast intersystem crossing in acetylacetone via femtosecond X-ray transient absorption at the carbon K-edge. *J. Am. Chem. Soc.* **139**, 16576–16583 (2017).
111. Lackner, F. et al. Direct observation of ring-opening dynamics in strong-field ionized selenophene using femtosecond inner-shell absorption spectroscopy. *J. Chem. Phys.* **145**, 234313 (2016).
112. Chatterley, A. S., Lackner, F., Neumark, D. M., Leone, S. R. & Gessner, O. Tracking dissociation dynamics of strong-field ionized 1,2-dibromoethane with femtosecond XUV transient absorption spectroscopy. *Phys. Chem. Chem. Phys.* **18**, 14644–14653 (2016).
113. Chatterley, A. S. et al. Dissociation dynamics and electronic structures of highly excited ferrocenium ions studied by femtosecond XUV absorption spectroscopy. *J. Phys. Chem. A* **120**, 9509–9518 (2016).
114. Attar, A. R., Bhattacherjee, A. & Leone, S. R. Direct observation of the transition-state region in the photodissociation of CH_3I by femtosecond extreme ultraviolet transient absorption spectroscopy. *J. Phys. Chem. Lett.* **6**, 5072–5077 (2015).
115. Popmintchev, T. et al. Bright coherent ultrahigh harmonics in the keV X-ray regime from mid-infrared femtosecond lasers. *Science* **336**, 1287–1291 (2012).
116. Biegert, J. Attosecond dispersive soft x-ray absorption fine structure spectroscopy. APS Physics http://meetings.aps.org/Meeting/DAMOP18/Session/K05.2 (2017).
117. Cavalleri, A. et al. Band-selective measurements of electron dynamics in VO_2 using femtosecond near-edge X-ray absorption. *Phys. Rev. Lett.* **95**, 067405 (2005).
118. McCusker, J. K. et al. Subpicosecond $^1MLCT \rightarrow {}^5T_2$ intersystem crossing of low-spin polypyridyl ferrous complexes. *J. Am. Chem. Soc.* **115**, 298–307 (1993).
119. Monat, J. E. & McCusker, J. K. Femtosecond excited-state dynamics of an iron(II) polypyridyl solar cell sensitizer model. *J. Am. Chem. Soc.* **122**, 4092–4097 (2000).
120. Gawelda, W. et al. Ultrafast nonadiabatic dynamics of $[Fe^{II}(bpy)_3]^{2+}$ in solution. *J. Am. Chem. Soc.* **129**, 8199–8206 (2007).
121. Létard, J.-F., Guionneau, P. & Goux-Capes, L. in Spin Crossover in Transition Metal Compounds III (eds Gütlich, P. & Goodwin, H. A.) 221–249 (Springer Berlin, 2004).
122. Brady, C., McGarvey, J. J., McCusker, J. K., Toftlund, H. & Hendrickson, D. N. in Spin Crossover in Transition Metal Compounds III (eds Gütlich, P. & Goodwin, H. A.) 1–22 (Springer Berlin, 2004).
123. Khalil, M. et al. Picosecond X-ray absorption spectroscopy of a photoinduced iron(II) spin crossover reaction in solution. *J. Phys. Chem. A* **110**, 38–44 (2006).
124. Van Kuiken, B. E. et al. Probing the electronic structure of a photoexcited solar cell dye with transient X-ray absorption spectroscopy. *J. Phys. Chem. Lett.* **3**, 1695–1700 (2012).
125. Kim, C. D., Pillet, S., Wu, G., Fullagar, W. K. & Coppens, P. Excited-state structure by time-resolved X-ray diffraction. *Acta Crystallograph. A* **58**, 133–137 (2002).
126. Yasuda, N., Kanazawa, M., Uekusa, H. & Ohashi, Y. Excited-state structure of a platinum complex by X-ray analysis. *Chem. Lett.* **31**, 1132–1133 (2002).
127. Ozawa, Y. et al. Photoexcited crystallography of diplatinum complex by multiple-exposure IP method. *Chem. Lett.* **32**, 62–63 (2002).
128. Yasuda, N., Uekusa, H. & Ohashi, Y. X-ray analysis of excited-state structures of the diplatinum complex anions in five crystals with different cations. *Bull. Chem. Soc. Japan* **77**, 933–944 (2004).
129. Novozhilova, I. V., Volkov, A. V. & Coppens, P. Theoretical analysis of the triplet excited state of the $[Pt_2(H_2P_2O_5)_4]^{4-}$ ion and comparison with time-resolved X-ray and spectroscopic results. *J. Am. Chem. Soc.* **125**, 1079–1087 (2003).
130. Lockard, J. V. et al. Triplet excited state distortions in a pyrazolate bridged platinum dimer measured by X-ray transient absorption spectroscopy. *J. Phys. Chem. A* **114**, 12780–12787 (2010).
131. Haldrup, K. et al. Bond shortening (1.4 Å) in the singlet and triplet excited states of $[Ir_2(dimen)_4]^{2+}$ in solution determined by time-resolved X-ray scattering. *Inorg. Chem.* **50**, 9329–9336 (2011).
132. Marinellia, A. et al. Experimental demonstration of a single-spike hard-X-ray free-electron laser starting from noise. *Appl. Phys. Lett.* **111**, 151101 (2017).
133. Elkins, M. H., Williams, H. L., Shreve, A. T. & Neumark, D. M. Relaxation mechanism of the hydrated electron. *Science* **342**, 1496–1499 (2013).
134. Faubel, M., Schlemmer, S. & Toennies, J. A molecular beam study of the evaporation of water from a liquid jet. *Z. Phys. D Atoms Mol. Clusters* **10**, 269–277 (1988).
135. Faubel, M., Steiner, B. & Toennies, J. P. Photoelectron spectroscopy of liquid water, some alcohols, and pure nonane in free micro jets. *J. Chem. Phys.* **106**, 9013–9031 (1997).
136. Faubel, M., Siefermann, K. R., Liu, Y. & Abel, B. Ultrafast soft X-ray photoelectron spectroscopy at liquid water microjets. *Acc. Chem. Res.* **45**, 120–130 (2012).
137. Siefermann, K. R. & Abel, B. The hydrated electron: a seemingly familiar chemical and biological transient. *Angew. Chem. Int. Ed.* **50**, 5264–5272 (2011).
138. Fattahi, H. et al. Third-generation femtosecond technology. *Optica* **1**, 45–63 (2014).
139. Bostedt, C. et al. Ultrafast X-ray scattering of xenon nanoparticles: Imaging transient states of matter. *Phys. Rev. Lett.* **108**, 093401 (2012).
140. Rupp, D. et al. Coherent diffractive imaging of single helium nanodroplets with a high harmonic generation source. *Nat. Commun.* **8**, 493 (2017).
141. Bordiga, S., Groppo, E., Agostini, G., van Bokhoven, J. A. & Lamberti, C. Reactivity of surface species in heterogeneous catalysts probed by in situ X-ray absorption techniques. *Chem. Rev.* **113**, 1736–1850 (2013).
142. Fleischer, A., Kfir, O., Diskin, T., Sidorenko, P. & Cohen, O. Spin angular momentum and tunable polarization in high-harmonic generation. *Nat. Photon.* **8**, 543–549 (2014).
143. Fan, T. et al. Bright circularly polarized soft X-ray high harmonics for X-ray magnetic circular dichroism. *Proc. Natl Acad. Sci.* **112**, 14206–14211 (2015).
144. Beaulieu, S. et al. Attosecond-resolved photoionization of chiral molecules. *Science* **358**, 1288–1294 (2017).
145. Kfir, O. et al. Nanoscale magnetic imaging using circularly polarized high-harmonic radiation. *Sci. Adv.* **3**, eaao4641 (2017).
146. Chapman, H. N. et al. Femtosecond X-ray protein nanocrystallography. *Nature* **470**, 73–77 (2011).
147. Neutze, R., Wouts, R., van der Spoel, D., Weckert, E. & Hajdu, J. Potential for biomolecular imaging with femtosecond X-ray pulses. *Nature* **406**, 752–757 (2000).
148. Young, L. et al. Femtosecond electronic response of atoms to ultra-intense X-rays. *Nature* **466**, 56 (2010).
149. Kuleff, A. I., Kryzhevoi, N. V., Pernpointner, M. & Cederbaum, L. S. Core ionization initiates

subfemtosecond charge migration in the valence shell of molecules. *Phys. Rev. Lett.* **117**, 093002 (2016).
150. Mukamel, S., Healion, D., Zhang, Y. & Biggs, J. D. Multidimensional attosecond resonant X-ray spectroscopy of molecules: lessons from the optical regime. *Annu. Rev. Phys. Chem.* **64**, 101–127 (2013).
151. Cao, W., Warrick, E. R., Fidler, A., Leone, S. R. & Neumark, D. M. Near-resonant four-wave mixing of attosecond extreme-ultraviolet pulses with near-infrared pulses in neon: detection of electronic coherences. *Phys. Rev. A* **94**, 021802 (2016).
152. Cao, W., Warrick, E. R., Fidler, A., Neumark, D. M. & Leone, S. R. Noncollinear wave mixing of attosecond XUV and few-cycle optical laser pulses in gas-phase atoms: toward multidimensional spectroscopy involving XUV excitations. *Phys. Rev. A* **94**, 053846 (2016).
153. Ding, T. et al. Time-resolved four-wave-mixing spectroscopy for inner-valence transitions. *Opt. Lett.* **41**, 709–712 (2016).
154. Glover, T. et al. X-ray and optical wave mixing. *Nature* **488**, 603 (2012).
155. Lam, R. K. et al. Soft X-ray second harmonic generation as an interfacial probe. *Phys. Rev. Lett.* **120**, 023901 (2018).
156. Takahashi, E., Nabekawa, Y., Otsuka, T., Obara, M. & Midorikawa, K. Generation of highly coherent submicrojoule soft X-rays by high-order harmonics. *Phys. Rev. A* **66**, 021802 (2002).
157. Sansone, G., Poletto, L. & Nisoli, M. High-energy attosecond light sources. *Nat. Photon.* **5**, 655 (2011).
158. Goulielmakis, E. et al. Attosecond control and measurement: lightwave electronics. *Science* **317**, 769–775 (2007).
159. Timmers, H. et al. Polarization-assisted amplitude gating as a route to tunable, high-contrast attosecond pulses. *Optica* **3**, 707–710 (2016).
160. Hädrich, S. et al. Single-pass high harmonic generation at high repetition rate and photon flux. *J. Phys. B Atom. Mol. Opt. Phys.* **49**, 172002 (2016).
161. Cingöz, A. et al. Direct frequency comb spectroscopy in the extreme ultraviolet. *Nature* **482**, 68 (2012).
162. Reid, D. T. et al. Roadmap on ultrafast optics. *J. Opt.* **18**, 093006 (2016).
163. Bressler, C. & Chergui, M. Ultrafast X-ray absorption spectroscopy. *Chem. Rev.* **104**, 1781–1812 (2004).
164. Kraus, P. M. & Wörner, H. J. Perspectives of attosecond spectroscopy for the understanding of fundamental electron correlations. *Angew. Chem. Int. Ed.* **57**, 5228-5247 (2018).
165. Buades, B. et al. Dispersive soft x-ray absorption fine-structure spectroscopy in graphite with an attosecond pulse. *Optica* **5**, 502–506 (2018).
166. Wörner, H. J. et al. Charge migration and charge transfer in molecular systems. *Struct. Dyn.* **4**, 061508 (2017).

Acknowledgements
We acknowledge funding from the Air Force Office of Scientific Research (AFOSR) (grant nos. FA9550-15-1-0037 and FA9550-14-1-0154), the Army Research Office (ARO) (WN911NF- 14-1-0383), the Office of Assistant Secretary of Defense for Research and Engineering through a National Security Science and Engineering Faculty Fellowship (NSSEFF), the W. M. Keck Foundation, the Defense Advanced Research Projects Agency PULSE program through grant W31P4Q-13-1-0017 and the National Science Foundation (NSF) through grants CHE-1361226 and CHE-1660417, and through a Foundation Major Research Instrumentation (NSF MRI) grant #1624322. Further funding was provided by the U.S. Department of Energy, Office of Science, Office of Basic Energy Sciences, Atomic, Molecular and Optical Sciences Program, Physical Chemistry of Inorganic Nanostructures Program and Gas Phase Chemical Physics Program under contract no. DE-AC02-05-CH11231. P.M.K. acknowledges support from the Swiss National Science Foundation (grant nos. P2EZP2 165252 and P300P2 174293). M.Z. acknowledges support from the Humboldt Foundation. S.K.C. is supported by the Department of Energy, Office of Energy Efficiency and Renewable Energy (EERE) Postdoctoral Research Award under the EERE Solar Energy Technologies Office.

Author contributions
All authors contributed, reviewed and edited the manuscript. P.M.K., M.Z., S.K.C. and S.R.L. researched data and discussed the content of the manuscript. P.M.K. and S.R.L wrote the manuscript.

Competing interests
The authors declare that they have no competing financial interests.

Publisher's note
Springer Nature remains neutral with regard to jurisdictional claims in published maps and institutional affiliations.

Reviewer information
Nature Reviews Chemistry thanks G. Cerullo and L. X. Chen for their contribution to the peer review of this work.

RELATED LINKS
European XFEL facilities comparison: https://www.xfel.eu/facility/comparison/index_eng.html